Crystal Structures of $\{P(CH_3)_4\}_2CuCl_4$ in Phases I, II and III

Yasuo NISHIJIMA* and Hiroyuki MASHIYAMA

Department of Physics, Faculty of Science, Yamaguchi University, Yamaguchi 753-8512

(Received July 10, 2000)

The crystal structures of $\{P(CH_3)_4\}_2CuCl_4$ in phase I, II and III are determined by single crystal X-ray diffractometry. The phase I is isomorphous to the normal phase of $\{N(CH_3)_4\}_2ZnCl_4$-type crystal, though the $CuCl_4$ tetrahedron is fairly distorted from the regular tetrahedral shape. The incommensurate phase II is refined by the use of the 4-dimensional superspace group. The second harmonics of the modulation is comparably strong as the primary modulation at 360K. The incommensurate structure is compared with the room temperature phase III, where the cell dimension along the c axis is tripled. The structural transition sequence is discussed in connection to the size of tetrahedral monovalent cation.

KEYWORDS: phase transition, incommensurate crystal, structure analysis, $\{P(CH_3)_4\}_2CuCl_4$

§1. Introduction

Many compounds in the A_2BX_4 family (where A is a monovalent cation and BX_4 is a divalent tetrahedral anion), the most studied example being K_2SeO_4,[1,2] exist in an orthorhombic phase (pseudo-hexagonal phase, $b/a \approx \sqrt{3}$) at high temperature, but undergo a transition to an incommensurate phase at low temperature. The modulation wave vector of the satellite reflections varies with temperature in the incommensurate phase, but locks-into a constant value on entering a commensurate phase at lower temperature.

Among the A_2BX_4 family, those compounds with the tetramethylammonium (TMA: $N(CH_3)_4$) group as the monovalent cation constitute an important subfamily for which a common pressure-temperature phase diagram has been proposed, where B is a metallic ion (Zn, Fe, Co, Ni) and X is halogen (Cl and Br).[3,4] Nevertheless, and apparently as a general rule, compounds with the central atom of the anion tetrahedron being Cu present special features and cannot be put in such a phase diagram. As an additional difficulty, CuX_4 testrahedra show a strong Jahn-Teller distortion which probably contributes to their unusual phase-transition scheme.[5,6]

It has been argued, from the characteristic behavior of bromide compounds as well as the experimental results for deuterated derivatives, that the size of cation relative to anion plays an

* Present address: Yamaguchi Pref. Fisheries High School, Senzaki 1002, Nagato, Yamaguchi 759-4106.

important role in the stability range of the phases of these materials.[3,7] This observed variation of phase behavior with change in the size of cation or anion prompted us to synthesize a series of analogous compounds using the larger tetramethylphosphonium (TMP: $P(CH_3)_4$) cation.[8]

This paper reports studies on the first compound in this series, $(TMP)_2CuCl_4$.[9] The phase sequence of $(TMP)_2CuCl_4$ can be schematized as Table I, where the transition temperatures are referred to the papers so far reported.[8,9] The superspace group of phase II is determined in this report. All the crystal structures of phases I, II and III are determined by single crystal X-ray diffractometry at 385, 360 and 297K. The characteristics of the structure are discussed in comparison with related TMA-compounds.

§2. Experimentals

Single crystals of $(TMP)_2CuCl_4$ used in this study were supplied by Gesi of Iwaki Meisei University. Stoichiometric amounts of $P(CH_3)_4Cl$ and $CuCl_2$ were mixed in 1-propanol. The resulting yellow precipitate was filtered and recrystallized from water.[9]

Intensity data collection was made on a 4-circle diffractometer(HUBER-AXC) with Mo Kα (λ=0.7107Å) radiation monochromated by graphite (001). The crystal data are summarized in Table II. The crystal structures were analyzed by the program system AXS89.[10] REMOS85 written by A. Yamamoto was employed for the least-squares calculations of the incommensurate structure.[11]

§3. Modulation Vector and Satellite Reflection Intensity

With increasing temperature, $(TMP)_2CuCl_4$ transforms from the commensurate $P2_1/c$ phase (phase III) to the incommensurate phase (phase II) at T_c=350K, and to the normal $Pmcn$ phase (phase I) at T_i=382K. The modulation wave vector q decreases discontinuously from the lock-in value of $\frac{1}{3}c_0^*$ at T_c to the incommensurate value of about $0.25c_0^*$, and then decreases continuously to $0.19c_0^*$ at T_i. The temperature variation of q determined from $(1\ 3\ 1-q)$ is shown in Fig. 1. The thermal hysteresis of q is tiny within the incommensurate phase in contradict to the early study.[9] The lock-in transition is the first order one with accompanying thermal hysteresis of a few kelvin.

Figure 2 represents the intensity of two first-order satellite reflections and one second-order one on heating as a function of temperature. The phase I-II transition is the second order one at $T = T_i$. The solid lines correspond to a function $I = c(T_i - T)^{2\beta}$, $T < T_i$, with c and 2β as fitting parameters. The value of 2β is estimated as 0.57 in this experiment, but it has been predicted on theoretical grounds, based on a three-dimensional xy model, to be 0.70.[2] One of the causes of discrepancy could be that the high-order terms increase rapidly as temperature departs from T_i. The variation of 2β on individual first-order reflections, reported by the early study,[9] is not found in our experiment. The power index for the secondary satellite $(0\ 4\ 1-2q)$ is fitted to be 1.47(7).

§4. The Normal Phase Structure

Intensities were measured at 385K. Range of hkl: -11$\leq h \leq$0, -20$\leq k \leq$19, -16$\leq l \leq$16. A total of 4690 reflections were collected, and 989 unique reflections with the criterion $F > 7\sigma(F)$ were devoted to analysis. Absorption correction for spherical specimen was carried out by Gaussian integration.

In the split atom model,[12] each atom occupies two positions related by the mirror symmetry $\{\sigma_x|a/2\}$ with an equal probability. Refinements with anisotropic thermal parameters for all atoms gave an R-factor of 0.050 and an S-factor of 1.55. In the displacive model, three pairs of Cl(3) and Cl(4), C(3) and C(4), and C(7) and C(8) are related by the mirror symmetry, and other 9 atoms sit on the mirror plane. Refinements with anisotropic thermal parameters for all atoms gave the R-factor of 0.080 and the S-factor of 2.24. It is clear that the crystal structure is well described by the split atom model.

Final atomic coordinates and equivalent isotropic thermal parameters are given in Table III for the split atom model.[13] The crystal structure is plotted in Fig. 3. The ellipsoids represent the thermal parameters. Bond lengths and angles are listed in Table IV. The Cl-Cu-Cl bond angles range from 94.3° to 134.9°. The $CuCl_4$ adopts a flattened shape characteristic of the Jahn-Teller distortion, which also appears in the isomorphous compounds of $(TMA)_2CuCl_4$,[14] $(TMA)_2CuBr_4$[15] and $(TMP)_2CuBr_4$.[16] Each TMP tetrahedron shows a more homogeneous distribution of bond angles, and all the C-P-C bond angles can be covered by the interval $103.3° \sim 114.7°$, indicating a geometrical distortion smaller than that of $CuCl_4$.

Rotation angles R_a, R_b and R_c around the a, b and c axes for the $CuCl_4$ and TMP rigid groups in the split atom model, from the positions in the displacive model, that is, from the mean structure, are summarized in Table V. The $CuCl_4$ and $TMP(2)$ testrahedra are mostly rotated around the c-axis, while the $TMP(1)$ tetrahedron around the b-axis.

§5. The Incommensurate Structure

Intensities were measured at 360K. The value of wave vector was obtained as $q = 0.23c_0^*$, from the profile of scanned satellite reflections. Range of $hklm$: 0$\leq h \leq$10, 0$\leq k \leq$19, -15$\leq l \leq$15, -2$\leq m \leq$2. A total of 3487 reflections were collected, and 3243 reflections with the criterion $F > 6\sigma(F)$ were observed (1779 unique reflections). Absorption correction for spherical specimen was carried out by Gaussian integration. The systematic absence for collected reflections are compatible with $P(Pmcn) : (ss\overline{1})$ superspace group. Weak 33 reflections were removed at last because of their bad profiles in ω-scan.

Modulation harmonics are considered up to the same order as the order of the measured satellites, that is, second order. In this way, displacements for each atom are due to the constant term and first and second harmonics. The superspace group symmetry reduces the number of amplitudes to

be refined for atoms in special positions. The final R-factors are 0.073, 0.058, 0.097 and 0.306 for all, main(1714), first-order satellite(1409) and second-order satellite(87) reflections, respectively.[13] Here the numbers of each kind of reflections are given in parentheses.

Final atomic coordinates and equivalent isotropic thermal parameters are given in Table VI, where the basic positions R_0 correspond to those obtained by us in the displacive model for phase I at 385K. The structural modulation can be visualized in drawings of modulated rotations and modulated translations of the $CuCl_4$ and TMP rigid groups. For these groups, rotations R_a, R_b and R_c around the a, b and c axes, as a function of the internal coordinate t, can be fitted to Fourier series. The results are shown in Figs. 4 and 5. The double harmonic character shown in the R_a rotation and the single harmonic characters shown in the R_b and R_c rotations (see Fig. 4) is attributed to the superspace group symmetry. But the associated translation motion T of the rigid groups must show a complementary character, that is, T_a is single, whereas T_b and T_c are double harmonics (see Fig. 5). For these groups, the most important rotation is R_c. In $(TMA)_2BX_4$ and $(TMP)_2BX_4$ (where B is not Cu but Zn, Co, etc. and X is halogen), R_c rotations are in phase for the BX_4 and $TMA(1)$ (or $TMP(1)$).[17] But in $(TMP)_2CuCl_4$, R_c rotations show less-definite phase relations. Such relation also holds in $(TMA)_2CuBr_4$.[18]

§6. The Locked-in Structure

Intensities were measured at 297K. Range of hkl: $-11 \leq h \leq 0$, $0 \leq k \leq 19$, $-45 \leq l \leq 45$. A total of 9783 reflections were collected, and 4423 unique reflections with the criterion $F > 7\sigma(F)$ were observed. Absorption correction for spherical specimen was carried out by Gaussian integration. Refinements with anisotropic thermal parameters for all atoms gave the R-factor of 0.048 (0.046 for 1673 main reflections and 0.049 for 2750 satellite reflections) and the S-factor of 4.10.[13]

The atomic parameters are given in Table VII. The projection of the structure on the $b-c$ plane is drawn in Fig. 6. The bond lengths and angles are listed in Table VIII.

For the $CuCl_4$ and TMP rigid groups, rotations R_a, R_b and R_c around the a, b and c axes and translation motion T_a, T_b and T_c, as a function of the internal coordinate t, can be fitted to Fourier series. The results are shown in Fig. 7 and Fig. 8. In comparison with phase II, the translations of $CuCl_4$ rigid group along the three axes increase their amplitude. The rotational modulations of $TMP(2)$ around the b- and c-axes change their phases relative to other modulation waves; the phase shifts are about $\Delta t \simeq 0.15$.

§7. Discussion

We have solved the crystal structures of all phases of $(TMP)_2CuCl_4$. The crystal structure of phase I is orthorhombic, space group $Pmcn$, with Z=4. The structure consists of tetrahedral $CuCl_4$ ions located on the mirror planes, bonded to TMP groups located on the same planes. The crystal structure of phase II is the incommensurate modulation of the basic structure, with the wave vector

$q = (1/3 - \delta)c_0^*$. The behavior of the first-order satellite intensities follows to the critical relation $(T - T_{\rm i})^{2\beta}$ with 2β=0.57(3). The crystal structure of phase III is monoclinic, space group $P12_1/c1$, with Z=12. The modulation waves in phases II and III can be fitted to sinusoidal functions. The phase relations of the modulation waves for the $CuCl_4$ and TMP rigid groups in phase III retain some similarity to those in phase II.

A compound of the TMZ_2BX_4 (here, TMZ is either TMA or TMP) type has a hexagonal network in which BX_4 testrahedra and TMZ testrahedra are arranged alternately when viewed from the c axis. When metallic ion B of the compound is not Cu, the distance between adjacent testrahedra in the hexagonal network is shortest and the network is strongly formed. As a result, regarding the modulation function of each tetrahedron for the rotation on the c axis (internal coordinates in the IC phase), BX_4 and the related TMZ have the same phase.

On the contrary, in $(TMA)_2CuBr_4$, the distance between the testrahedra which constitute the hexagonal network , i.e. $CuBr_4$-$TMA(1)$, is almost the same as the distance between $CuBr_4$ and $TMA(2)$. $CuBr_4$ is largely affected by $TMA(2)$, and so the hexagonal network is weakly formed. As a result, regarding the modulation function of each tetrahedron for the rotation about the c axis, BX_4 and the related TMZ have slightly different phases.

In $(TMA)_2CuBr_4$, the distance between $CuBr_4$ and $TMA(1)$ is 0.002Å shorter than the distance between $CuBr_4$ and $TMA(2)$. In $(TMA)_2CuCl_4$, the distance between $CuCl_4$ and $TMA(1)$ is 0.053Å longer than the distance between $CuCl_4$ and $TMA(2)$. In $(TMP)_2CuBr_4$, the distance between $CuBr_4$ and $TMP(1)$ is 0.109Å longer than the distance between $CuBr_4$ and $TMP(2)$. In $(TMP)_2CuCl_4$, the distance between $CuCl_4$ and $TMP(1)$ is 0.168Å longer than the distance between $CuCl_4$ and $TMP(2)$. In $(TMA)_2ZnCl_4$, the distance between $ZnCl_4$ and $TMA(1)$ is 0.197Å shorter than the distance between $ZnCl_4$ and $TMA(2)$.

Therefore, in tetramethylammonium compound (TMA_2BX_4 (B=Mn, Fe, Co, Zn; X=Cl, Br)), the distance between BX_4 and $TMA(1)$ is short, and the hexagonal network consisting of three BX_4's and three $TMA(1)$'s is formed strongly. Increasing the size of tetrahedron provides the same effect as applying hydrostatic pressure. Thus the temperature-pressure phase diagram is universal.[3,7)]

On the other hand, in a compound of the TMZ_2CuX_4 (X=Cl, Br) type, the distance between CuX_4 and $TMZ(1)$ is same as or longer than the distance between CuX_4 and $TMZ(2)$. Therefore, the hexagonal network consisting of three CuX_4's and three $TMZ(1)$'s is considered to be weakly formed. In addition, the degree of weakness depends on the element used, such as N, P, Cl and Br. Therefore, the chemical components of the TMZ_2CuX_4 type do not have common characteristics regarding to the hexagonal network. As a result, increasing the tetrahedron size does not provide the same effect as applying hydrostatic pressure, which means that the same temperature-pressure phase diagram is not applicable.

Although the basic structure is the hexagonal network, the CuX_4 regular tetrahedron is distorted by the Jahn-Teller effect in compounds of the TMZ_2CuX_4 (X=Cl, Br) type. The degree of distortion depends on the element used such as N, P, Cl, and Br and the strength of the hexagonal network also depends on the element used. For this reason, chemical compounds of the $(TMZ)_2CuX_4$ (X=Cl, Br) type show various characteristics that are not shown by chemical compounds of the $(TMA)_2BX_4$ (B=Mn, Fe, Co, Zn; X=Cl, Br).

Only a few crystal structures have been solved for $(TMP)_2CuBr_4$, $(TMA)_2CuCl_4$ or $(TMA)_2CuBr_4$ compounds in which the central atom of the anion is Cu; phase IV of $(TMP)_2CuBr_4$,[16] phase I of $(TMA)_2CuCl_4$,[14] phases I, II and III of $(TMA)_2CuBr_4$.[18] In order to understand quantitatively how Jahn-Teller distortion or the difference in the sizes of cation or anion will influence the characters of $(TMP)_2CuCl_4$ which has been found in this study, the crystal structures of all phases of these compounds are desired to be solved.

Acknowledgements

The authors are grateful to Prof. Gesi, Iwaki Meisei University, for his kindness to supply single crystals. They would also like to thank colleagues in their department who have made a lot of discussions.

1) M. Iizumi, J. D. Axe, G. Shirane and K. Shimaoka: Phys. Rev. B**15** (1977) 4392.
2) J. D. Axe, M. Iizumi and G. Shirane: *Incommensurate Phases in Dielectrics II*, ed. by R. Blinc and A. P. Levanyuk (North-Holland, Amsterdam, 1986) p.1.
3) H. Shimizu, N. Abe, N. Kokubo, N. Yasuda, S. Fujimoto, T. Yamaguchi and S. Sawada: Solid State Commun. **34** (1980) 363.
4) E. Colla, R. Muralt, H. Arend, R. Perret, R. Godefroy and C. Dumas: Solid State Commun. **52** (1984) 1033.
5) K. Gesi and M. Iizumi: J. Phys. Soc. Jpn. **48** (1980) 1775.
6) K. Gesi and K. Ozawa: J. Phys. Soc. **51** (1982) 2205.
7) K. Gesi: Ferroelectrics **66** (1986) 269.
8) M. R. Pressprich, M. R. Bond and R. D. Willet: Phys. Rev. B**43** (1991) 13549.
9) M. R. Pressprich, M. R. Bond and R. D. Willet and M. A. White: Phys. Rev. B**39** (1989) 3453.
10) H. Mashiyama: J. Phys. Soc. Jpn. **60** (1991) 180.
11) A. Yamamoto: Acta Cryst. A**38** (1982) 82.
12) J. R. Wiesner, R. C. Srivastava, C. H. L. Kennard, M. DiVaira and E. C. Lingafelter: Acta Cryst. **23** (1967) 565.
13) Lists of structure data have been deposited with http://cryst.instr.yamaguchi-u.ac.jp/20002.
14) R. Clay, J. Murray-Rust and P. Murray-Rust: Acta Cryst. B**31** (1975) 289.
15) K. Hasebe, H. Mashiyama and S. Tanisaki: Jan. J. App. Phys. **24** (1985) 758.
16) G. Madariaga, M. M. Alberdi and F. J. Zuniga: Acta Cryst. C**46** (1990) 2363.
17) G. Madariaga, F. J. Zuniga, J. M. Perez-Mato and M. J. Tello: Acta Cryst. B**43** (1987) 356.
18) G. Madariaga, F. J. Zuniga and W. A. Paciorek: Acta Cryst. B**46** (1990) 620.

Fig. 1. Temperature dependence of the modulation wave number of $\{P(CH_3)_4\}_2CuCl_4$ on heating ($\circ$) and on cooling($\times$).

Fig. 2. Temperature dependence of the integrated intensity of two first-order satellites and one second-order satellite of $\{P(CH_3)_4\}_2CuCl_4$ on cooling. The scale of the intensity is in arbitrary units. The solid curves are fitted to the observed data by least-squares methods.

Fig. 3. Projections of the crystal structure of $\{P(CH_3)_4\}_2CuCl_4$ at 385K along the c and a axes. The counterpart of configuration related by the mirror symmetry is not drawn to avoid the complexity.

Fig. 4. Rotational modulations as a function of the internal coordinate t in the incommensurate phase of $\{P(CH_3)_4\}_2CuCl_4$ at 360K. R_a, R_b and R_c are rotations in degree around a, b and c axes.

Fig. 5. Translational modulations as a function of the internal coordinate t in the incommensurate phase of $\{P(CH_3)_4\}_2CuCl_4$ at 360K. T_a, T_b and T_c are translations in angstrom along a, b and c axes.

Fig. 6. Projection on the $b-c$ plane of the crystal structure of $\{P(CH_3)_4\}_2CuCl_4$ at 297K in phase III.

Fig. 7. Rotational modulation patterns in the commensurate phase III of $\{P(CH_3)_4\}_2CuCl_4$ at 297K. R_a, R_b and R_c are rotations in degree around a, b and c axes. The internal coordinate t is the z parameter of atoms.

Fig. 8. Translational modulation patterns in the commensurate phase III of $\{P(CH_3)_4\}_2CuCl_4$ at 297K. T_a, T_b and T_c are translations in angstrom along a, b and c axes. The internal coordinate t is the z parameter of atoms.

Table I. Phase transition sequences in $\{A(CH_3)_4\}_2CuX_4$. Here A is either N or P and X is halogen atom. INC in space group column means incommensurate phase. $\boldsymbol{q}$ and $T_{\rm tr}$ are the modulation wave vector and the transition temperature [K], respectively.

			$\{P(CH_3)_4\}_2CuCl_4$		
Phase	III		II		I
Space Group	$P12_1/c1$		INC		$Pmcn$
$\boldsymbol{q}$	$\frac{1}{3}c_o^*$		$\sim \frac{1}{4}c_o^*$		0
$T_{\rm tr}$		350		382	

			$\{P(CH_3)_4\}_2CuBr_4$			
Phase	IV		III	II		I
Space Group	$P112_1/n$		$P2_1/b11$	INC		$Pmcn$
$\boldsymbol{q}$	0		$\frac{1}{2}b_o^*$	$\sim \frac{1}{2}b_o^*$		0
$T_{\rm tr}$		202		406	409	

			$\{N(CH_3)_4\}_2CuCl_4$			
Phase	IV		III	II		I
Space Group	$P112_1/n$		$P12_1/c1$	INC		$Pmcn$
$\boldsymbol{q}$	0		$\frac{1}{3}c_o^*$	$\sim \frac{1}{3}c_o^*$		0
$T_{\rm tr}$		247		293	299	

			$\{N(CH_3)_4\}_2CuBr_4$			
Phase	IV		III	II		I
Space Group	$P12_1/c1$		$Pbc2_1$	INC		$Pmcn$
$\boldsymbol{q}$	0		$\frac{1}{2}b_o^*$	$\sim \frac{1}{2}b_o^*$		0
$T_{\rm tr}$		236		240	471	

Table II. Crystal data of $\{P(CH_3)_4\}_2CuCl_4$.

Phase	III	II	I
Crystal system	Monoclinic	Orthorhombic	Orthorhombic
Space group	$P12_1/c1$	$P(Pmcn):(ss\overline{1})$	$Pmcn$
Formula unit	12	4(mean structure)	4
Lattice parameter(Å)			
a	9.255(2)	9.297(2)	9.298(3)
b	15.574(2)	15.652(2)	15.685(6)
c	37.594(4)	12.645(2)	12.781(7)
Monoclinic angle(°)	β=90.27(1)	—	—
Volume(Å^3)	5418(1)	1840(1)	1864(1)
Measured range 2θ(°)	55	60	60
Index range			
h	-11∼11	0∼10	-11∼ 0
k	0∼19	0∼19	-20∼19
l	-45∼45	-15∼15	-16∼16
m		-2∼ 2	
Measurement temperature(K)	297	360	385
Number of measured reflections	9783	3487	4690
Number of unique reflections	4423($F > 7\sigma(F)$)	1779($F > 6\sigma(F)$)	989($F > 7\sigma(F)$)
Number of parameters	407	172	137
Absorption coefficient (mm^{-1})	1.958	1.906	1.900
Crystal radius (mm)	0.16	0.24	0.23
Transmission factors	0.636 ∼ 0.640	0.518 ∼ 0.526	0.533 ∼ 0.540
Final R-factor	0.048	0.073	0.050
S-factor	4.10	-	1.55
Maximum deviation $(\Delta/\sigma)_{max}$	0.022	-	0.099
Residual electron density $\Delta\rho$ (e/Å^3)	$-0.36 \sim 0.52$	-	$-0.31 \sim 0.24$

Table III. Final atomic coordinates and equivalent isotropic thermal parameters(Å^2) with e.s.d.'s in parentheses for phase I at 385K of $\{P(CH_3)_4\}_2CuCl_4$. The multiplicity for all atoms is $\frac{1}{2}$ in the split atom model.

Atom	x	y	z	B_{eq}
Cu	.2652(2)	.39918(5)	.22697(6)	7.25(2)
Cl(1)	.2837(4)	.3604(2)	.0590(2)	12.2(1)
Cl(2)	.3032(3)	.5240(2)	.3073(2)	12.4(1)
Cl(3)	.4550(4)	.3288(2)	.2757(3)	14.4(1)
Cl(4)	.0309(3)	.3859(3)	.2541(3)	19.2(2)
P(1)	.2436(7)	.0869(1)	.1213(1)	7.22(5)
C(1)	.2845(10)	.1093(6)	.2582(5)	11.2(4)
C(2)	.2222(12)	-.0252(4)	.1006(6)	9.5(3)
C(3)	.3934(10)	.1257(6)	.0430(7)	9.8(3)
C(4)	.0783(10)	.1414(7)	.0864(7)	10.9(3)
P(2)	.2440(8)	.8414(1)	.5167(2)	7.56(5)
C(5)	.2793(12)	.7590(5)	.4198(7)	11.4(3)
C(6)	.1846(15)	.9334(6)	.4565(11)	19.8(6)
C(7)	.4145(10)	.8722(7)	.5713(9)	12.6(4)
C(8)	.1152(13)	.8082(8)	.6093(9)	15.8(5)

Table IV. Bond lengths(Å) and angles(°) of $CuCl_4$ and $P(CH_3)_4$ for phase I at 385K of $\{P(CH_3)_4\}_2CuCl_4$. The e.s.d's are given in parentheses.

Atom pair	Length	Atom pair	Length	Atom pair	Length
Cu-Cl(1)	2.238(3)	P(1)-C(1)	1.824(8)	P(2)-C(5)	1.820(9)
Cu-Cl(2)	2.238(3)	P(1)-C(2)	1.790(7)	P(2)-C(6)	1.725(11)
Cu-Cl(3)	2.173(4)	P(1)-C(3)	1.820(10)	P(2)-C(7)	1.798(12)
Cu-Cl(4)	2.215(4)	P(1)-C(4)	1.815(11)	P(2)-C(8)	1.762(13)
Bond pair	**Angle**	**Bond pair**	**Angle**	**Bond pair**	**Angle**
Cl(1)-Cu-Cl(2)	131.7(3)	C(1)-P(1)-C(2)	110.8(8)	C(5)-P(2)-C(6)	110.4(10)
Cl(1)-Cu-Cl(3)	94.3(2)	C(1)-P(1)-C(3)	107.7(8)	C(5)-P(2)-C(7)	107.2(10)
Cl(1)-Cu-Cl(4)	101.6(3)	C(1)-P(1)-C(4)	108.8(9)	C(5)-P(2)-C(8)	111.7(11)
Cl(2)-Cu-Cl(3)	100.6(2)	C(2)-P(1)-C(3)	109.4(9)	C(6)-P(2)-C(7)	103.3(11)
Cl(2)-Cu-Cl(4)	99.5(2)	C(2)-P(1)-C(4)	109.4(9)	C(6)-P(2)-C(8)	109.2(12)
Cl(3)-Cu-Cl(4)	134.9(5)	C(3)-P(1)-C(4)	110.7(10)	C(7)-P(2)-C(8)	114.7(13)

Table V. Rotation angles(°) R_a, R_b and R_c around the a, b and c axes for the $CuCl_4$ and TMP rigid groups in the split atom model, from the positions in displacive model for phase I at 385K of $\{P(CH_3)_4\}_2CuCl_4$.

Tetrahedron	R_a	R_b	R_c
$CuCl_4$	-0.6	-5.0	-13.2
$TMP(1)$	0.0	11.0	-4.4
$TMP(2)$	3.6	9.0	19.9

Table VI. Positional($\times 10^4$) and thermal parameters of $\{P(CH_3)_4\}_2CuCl_4$ of the incommensurate structure (phase II) at 360K. Positional parameters are given as $x = R_0 + A_0 + A_1\cos(2\pi t) + B_1\sin(2\pi t) + A_2\cos(4\pi t) + B_2\sin(4\pi t)$, where R_0 is the parameter of phase I of the displacive model, and t is the internal coordinate of the modulation.

Atom		R_0	A_0	A_1	B_1	A_2	B_2	B_{eq}(Å^2)
Cu	x	2500	0	-295(1)	93(2)	0	0	6.01(1)
	y	3994	-3(0)	0	0	-43(3)	13(4)	
	z	2266	-49(0)	0	0	17(5)	12(4)	
Cl(1)	x	2500	0	-255(6)	303(6)	0	0	9.8(2)
	y	3603	-36(2)	0	0	-54(10)	-16(9)	
	z	580	-45(1)	0	0	-71(12)	12(12)	
Cl(2)	x	2500	0	-822(6)	452(8)	0	0	9.7(2)
	y	5246	-12(1)	0	0	-16(6)	36(6)	
	z	3086	-37(2)	0	0	-48(8)	48(8)	
Cl(3)	x	367	-98(2)	-120(3)	-90(4)	-25(6)	21(7)	11.9(2)
	y	3534	31(2)	-372(3)	232(3)	16(5)	-129(5)	
	z	2662	-41(2)	57(3)	-261(3)	39(6)	87(6)	
P(1)	x	2500	0	-77(3)	1(3)	0	0	5.4(2)
	y	866	-15(1)	0	0	-63(11)	41(12)	
	z	1214	-28(1)	0	0	57(15)	83(15)	
C(1)	x	2500	0	251(20)	260(21)	0	0	8.3(7)
	y	1092	18(7)	0	0	95(30)	103(33)	
	z	2584	-26(7)	0	0	49(36)	-260(12)	
C(2)	x	2500	0	150(17)	38(17)	0	0	6.1(9)
	y	-262	-18(5)	0	0	-109(32)	-30(27)	
	z	1002	-9(7)	0	0	83(39)	293(20)	
C(3)	x	4069	1(7)	-255(12)	-177(11)	-35(25)	-80(22)	9.2(5)
	y	1326	-30(5)	110(8)	24(9)	21(20)	-87(18)	
	z	647	-50(6)	-154(11)	-221(11)	53(27)	-25(23)	
P(2)	x	2500	0	-87(4)	141(4)	0	0	6.1(1)
	y	8412	-5(1)	0	0	-11(10)	-13(12)	
	z	5163	-14(1)	0	0	56(15)	27(15)	
C(5)	x	2500	0	-402(20)	149(21)	0	0	9.0(9)
	y	7582	15(6)	0	0	34(36)	-87(27)	
	z	4211	-36(8)	0	0	175(39)	39(42)	
C(6)	x	2500	0	566(31)	887(27)	0	0	10.9(11)
	y	9324	6(7)	0	0	-12(23)	-22(21)	
	z	4460	49(12)	0	0	-94(35)	271(30)	
C(7)	x	4034	-43(9)	-258(14)	-143(14)	-58(23)	-164(24)	10.4(7)
	y	8466	-87(7)	-376(11)	-255(12)	43(16)	-20(15)	
	z	5870	44(6)	166(12)	257(12)	23(22)	51(20)	

Table VII. Final atomic coordinates and equivalent isotropic thermal parameters(Å^2) with e.s.d.'s in parentheses for phase III at 297K of $\{P(CH_3)_4\}_2CuCl_4$.

Atom	x	y	z	B_{eq}	Atom	x	y	z	B_{eq}
Cu(a)	.2077(1)	.39402(9)	.07363(3)	4.13(3)	P(b2)	.2690(3)	.8430(2)	.50466(8)	4.31(7)
Cl(a1)	.1866(4)	.3534(2)	.01659(8)	6.51(9)	C(b5)	.2939(14)	.7553(8)	.4745(4)	7.4(4)
Cl(a2)	.1669(4)	.5153(2)	.10496(9)	6.53(9)	C(b6)	.2024(15)	.9319(8)	.4793(4)	7.3(4)
Cl(a3)	.4490(3)	.3939(3)	.07660(10)	8.84(13)	C(b7)	.4387(12)	.8714(10)	.5254(3)	7.5(4)
Cl(a4)	.0263(4)	.3145(2)	.09524(9)	7.00(10)	C(b8)	.1401(12)	.8102(10)	.5382(3)	7.2(4)
P(a1)	.2358(3)	.0838(2)	.04039(7)	4.02(7)	Cu(c)	.2585(1)	.41169(8)	.73761(3)	4.17(3)
C(a1)	.2609(14)	.1037(10)	.0871(3)	7.6(4)	Cl(c1)	.2692(3)	.3604(2)	.68216(8)	6.58(9)
C(a2)	.2637(12)	-.0282(7)	.0309(3)	5.8(3)	Cl(c2)	.3050(4)	.5354(2)	.76719(9)	6.94(10)
C(a3)	.3683(12)	.1435(8)	.0155(3)	6.5(4)	Cl(c3)	.4432(4)	.3364(3)	.75978(9)	7.80(11)
C(a4)	.0552(10)	.1156(8)	.0287(3)	6.0(3)	Cl(c4)	.0189(3)	.4200(4)	.74049(10)	10.94(15)
P(a2)	.2166(3)	.8295(2)	.17066(8)	4.44(7)	P(c1)	.2579(3)	.0883(2)	.70658(7)	4.25(7)
C(a5)	.1928(14)	.7482(8)	.1370(3)	6.7(4)	C(c1)	.2891(14)	.1138(9)	.7528(3)	7.3(4)
C(a6)	.1668(21)	.9268(9)	.1513(5)	14.1(7)	C(c2)	.2670(14)	-.0263(8)	.7008(3)	6.6(4)
C(a7)	.3973(13)	.8342(12)	.1865(4)	9.3(5)	C(c3)	.3947(11)	.1368(8)	.6798(3)	6.8(4)
C(a8)	.0904(16)	.8084(13)	.2061(4)	11.6(6)	C(c4)	.0816(12)	.1278(9)	.6931(3)	6.9(4)
Cu(b)	.2852(1)	.39184(8)	.40809(3)	4.04(3)	P(c2)	.2651(3)	.8466(2)	.84000(8)	4.43(7)
Cl(b1)	.2401(4)	.3451(2)	.35274(8)	6.46(9)	C(c5)	.2386(16)	.7702(9)	.8043(3)	8.5(4)
Cl(b2)	.3414(4)	.5199(2)	.43282(9)	6.49(9)	C(c6)	.3566(15)	.9382(8)	.8228(4)	8.7(5)
Cl(b3)	.4962(3)	.3245(2)	.41754(9)	7.21(10)	C(c7)	.3774(14)	.7954(9)	.8732(3)	7.2(4)
Cl(b4)	.0611(3)	.3807(3)	.42872(10)	8.66(12)	C(c8)	.0955(11)	.8793(9)	.8587(3)	6.9(4)
P(b1)	.2583(3)	.0794(2)	.37055(7)	4.01(7)					
C(b1)	.2093(13)	.1173(9)	.4143(3)	6.6(4)					
C(b2)	.2487(14)	-.0357(7)	.3688(3)	5.9(3)					
C(b3)	.4378(11)	.1162(8)	.3600(3)	6.1(4)					
C(b4)	.1301(12)	.1211(8)	.3383(3)	6.1(3)					

Table VIII. Bond lengths(Å) and angles(°) of $CuCl_4$ and $P(CH_3)_4$ for phase III at 297K of $\{P(CH_3)_4\}_2CuCl_4$.

Atom pair	Length	Atom pair	Length	Atom pair	Length
Cu(a) - Cl(a1)	2.243 (3)	P(a1) - C(a1)	1.80 (1)	P(a2) - C(a5)	1.80 (1)
Cu(a) - Cl(a2)	2.259 (3)	P(a1) - C(a2)	1.80 (1)	P(a2) - C(a6)	1.74 (2)
Cu(a) - Cl(a3)	2.235 (3)	P(a1) - C(a3)	1.80 (1)	P(a2) - C(a7)	1.77 (1)
Cu(a) - Cl(a4)	2.241 (4)	P(a1) - C(a4)	1.80 (1)	P(a2) - C(a8)	1.81 (2)
Cu(b) - Cl(b1)	2.242 (3)	P(b1) - C(b1)	1.81 (1)	P(b2) - C(b5)	1.79 (1)
Cu(b) - Cl(b2)	2.260 (3)	P(b1) - C(b2)	1.80 (1)	P(b2) - C(b6)	1.79 (1)
Cu(b) - Cl(b3)	2.243 (3)	P(b1) - C(b3)	1.80 (1)	P(b2) - C(b7)	1.80 (1)
Cu(b) - Cl(b4)	2.224 (3)	P(b1) - C(b4)	1.81 (1)	P(b2) - C(b8)	1.81 (1)
Cu(c) - Cl(c1)	2.235 (3)	P(c1) - C(c1)	1.81 (1)	P(c2) - C(c5)	1.81 (1)
Cu(c) - Cl(c2)	2.265 (4)	P(c1) - C(c2)	1.80 (1)	P(c2) - C(c6)	1.78 (1)
Cu(c) - Cl(c3)	2.231 (4)	P(c1) - C(c3)	1.79 (1)	P(c2) - C(c7)	1.81 (1)
Cu(c) - Cl(c4)	2.225 (3)	P(c1) - C(c4)	1.81 (1)	P(c2) - C(c8)	1.80 (1)
Bond pair	**Angle**	**Bond pair**	**Angle**	**Bond pair**	**Angle**
Cl(a1)-Cu(a)-Cl(a2)	136.1(4)	C(a1)-P(a1)-C(a2)	110(1)	C(a5)-P(a2)-C(a6)	107(1)
Cl(a1)-Cu(a)-Cl(a3)	97.5(2)	C(a1)-P(a1)-C(a3)	110(1)	C(a5)-P(a2)-C(a7)	112(1)
Cl(a1)-Cu(a)-Cl(a4)	97.4(2)	C(a1)-P(a1)-C(a4)	108(1)	C(a5)-P(a2)-C(a8)	108(1)
Cl(a2)-Cu(a)-Cl(a3)	98.3(2)	C(a2)-P(a1)-C(a3)	107(1)	C(a6)-P(a2)-C(a7)	111(2)
Cl(a2)-Cu(a)-Cl(a4)	98.4(2)	C(a2)-P(a1)-C(a4)	111(1)	C(a6)-P(a2)-C(a8)	107(2)
Cl(a3)-Cu(a)-Cl(a4)	137.0(5)	C(a3)-P(a1)-C(a4)	111(1)	C(a7)-P(a2)-C(a8)	111(1)
Cl(b1)-Cu(b)-Cl(b2)	135.2(4)	C(b1)-P(b1)-C(b2)	110(1)	C(b5)-P(b2)-C(b6)	107(1)
Cl(b1)-Cu(b)-Cl(b3)	98.8(2)	C(b1)-P(b1)-C(b3)	109(1)	C(b5)-P(b2)-C(b7)	110(1)
Cl(b1)-Cu(b)-Cl(b4)	97.4(2)	C(b1)-P(b1)-C(b4)	109(1)	C(b5)-P(b2)-C(b8)	108(1)
Cl(b2)-Cu(b)-Cl(b3)	98.6(2)	C(b2)-P(b1)-C(b3)	111(1)	C(b6)-P(b2)-C(b7)	110(1)
Cl(b2)-Cu(b)-Cl(b4)	98.0(2)	C(b2)-P(b1)-C(b4)	108(1)	C(b6)-P(b2)-C(b8)	111(1)
Cl(b3)-Cu(b)-Cl(b4)	136.1(4)	C(b3)-P(b1)-C(b4)	110(1)	C(b7)-P(b2)-C(b8)	110(1)
Cl(c1)-Cu(c)-Cl(c2)	138.8(5)	C(c1)-P(c1)-C(c2)	109(1)	C(c5)-P(c2)-C(c6)	109(1)
Cl(c1)-Cu(c)-Cl(c3)	97.1(2)	C(c1)-P(c1)-C(c3)	110(1)	C(c5)-P(c2)-C(c7)	107(1)
Cl(c1)-Cu(c)-Cl(c4)	96.6(2)	C(c1)-P(c1)-C(c4)	110(1)	C(c5)-P(c2)-C(c8)	111(1)
Cl(c2)-Cu(c)-Cl(c3)	96.9(2)	C(c2)-P(c1)-C(c3)	109(1)	C(c6)-P(c2)-C(c7)	109(1)
Cl(c2)-Cu(c)-Cl(c4)	96.5(2)	C(c2)-P(c1)-C(c4)	110(1)	C(c6)-P(c2)-C(c8)	109(1)
Cl(c3)-Cu(c)-Cl(c4)	140.7(5)	C(c3)-P(c1)-C(c4)	110(1)	C(c7)-P(c2)-C(c8)	111(1)

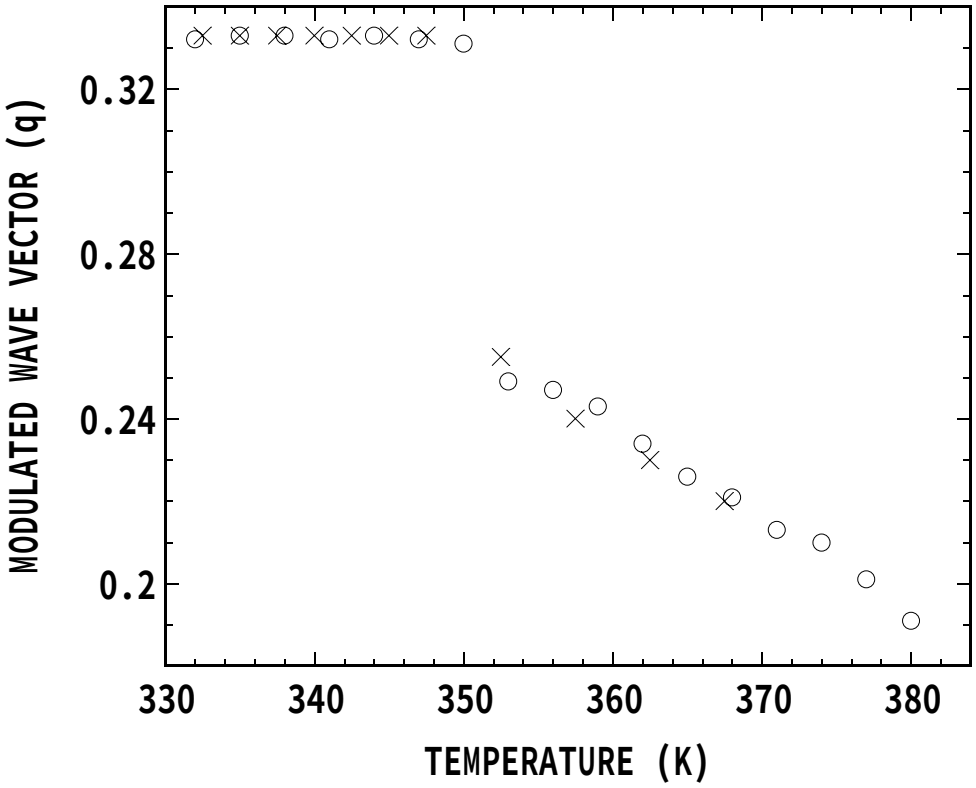
MODULATED WAVE VECTOR (q)
0.32
0.28
0.24
0.2
330
340
350
360
370
380
TEMPERATURE (K)

Fig. 1.

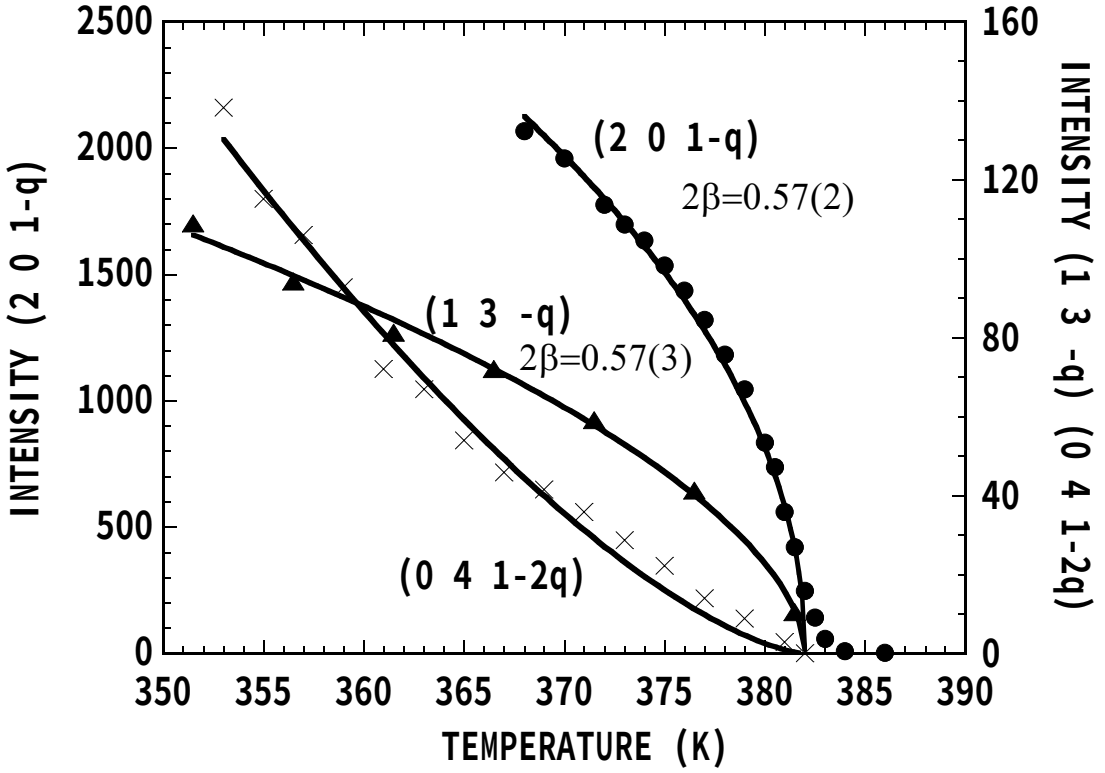
INTENSITY (2 0 1-q)
INTENSITY (1 3 -q) (0 4 1-2q)
2500
2000
1500
1000
500
0
160
120
80
40
0
350
355
360
365
370
375
380
385
390
TEMPERATURE (K)
(2 0 1-q)
2β=0.57(2)
(1 3 -q)
2β=0.57(3)
(0 4 1-2q)

Fig. 2.

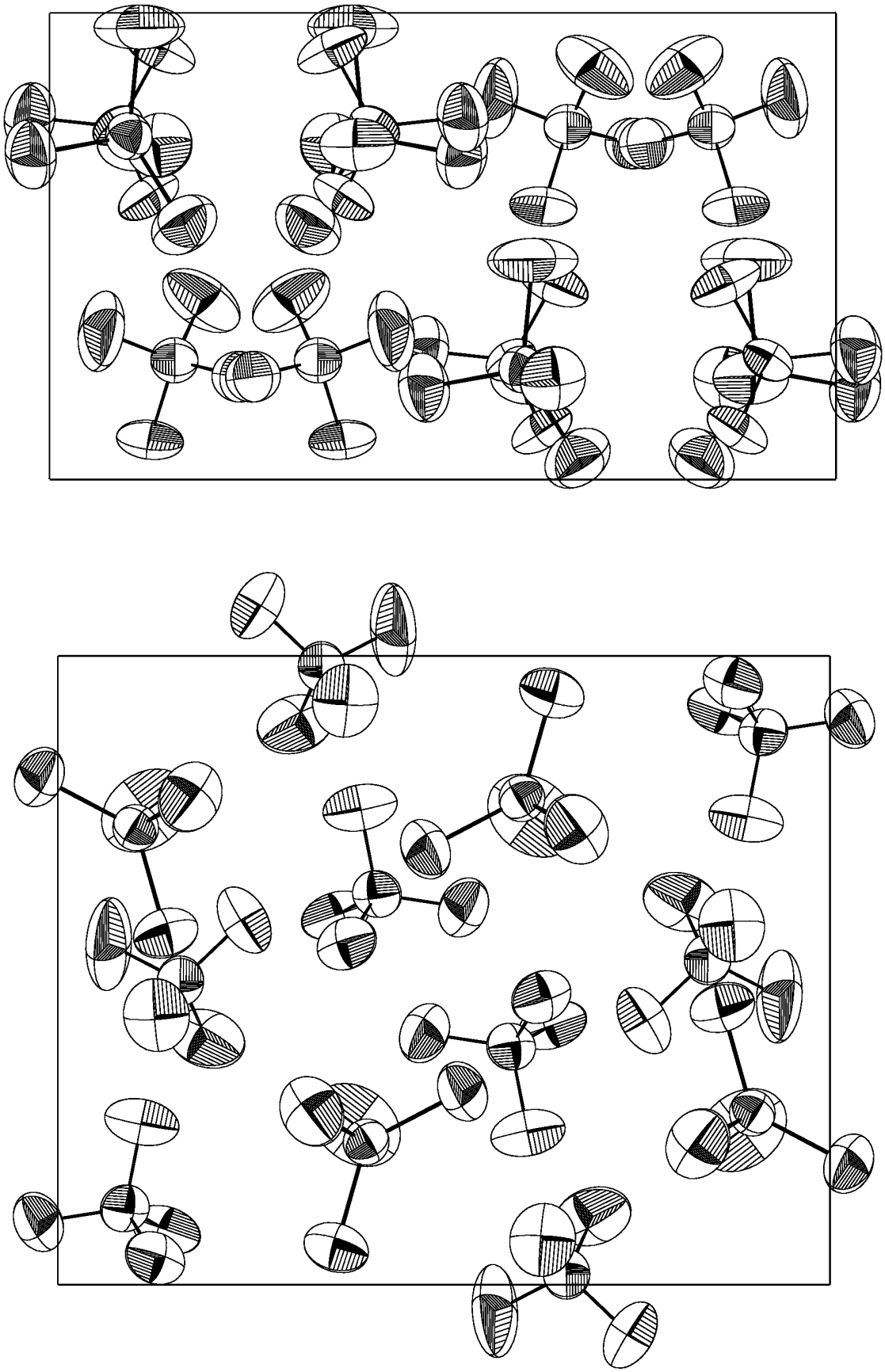

Fig. 3.

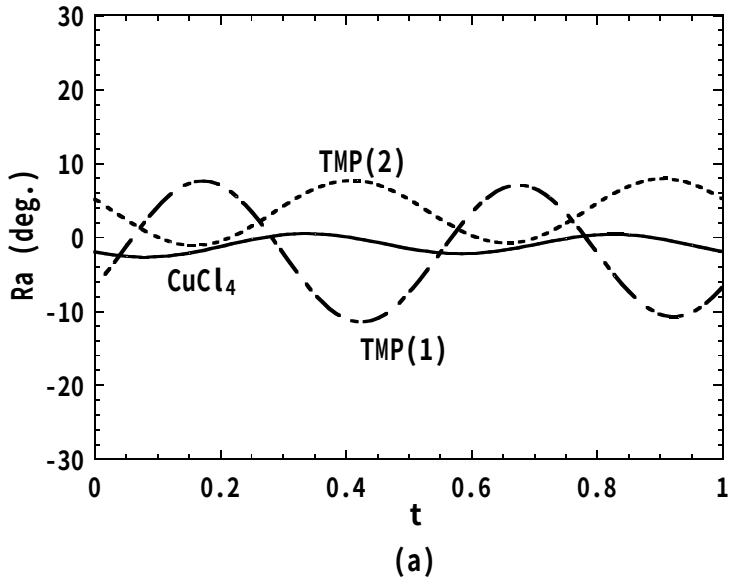
30
20
10
0
-10
-20
-30
Ra (deg.)
TMP(2)
CuCl4
TMP(1)
0
0.2
0.4
0.6
0.8
1
t
(a)

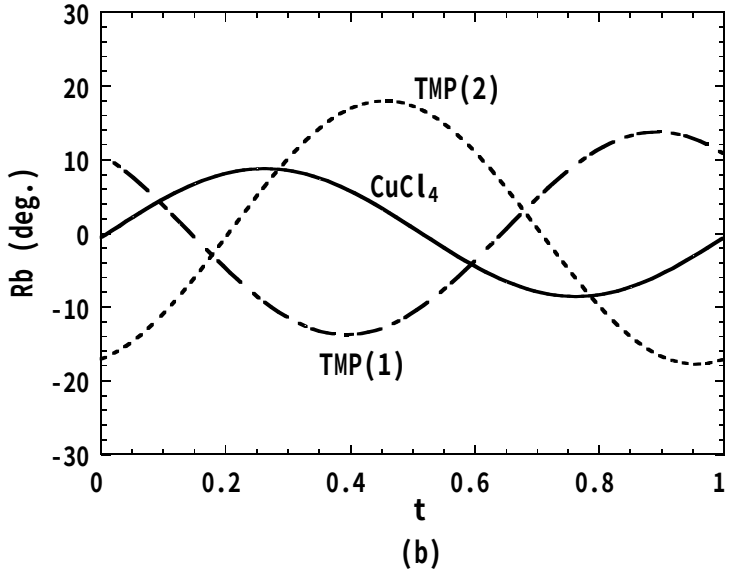
30
20
10
0
-10
-20
-30
Rb (deg.)
TMP(2)
CuCl4
TMP(1)
0
0.2
0.4
0.6
0.8
1
t
(b)

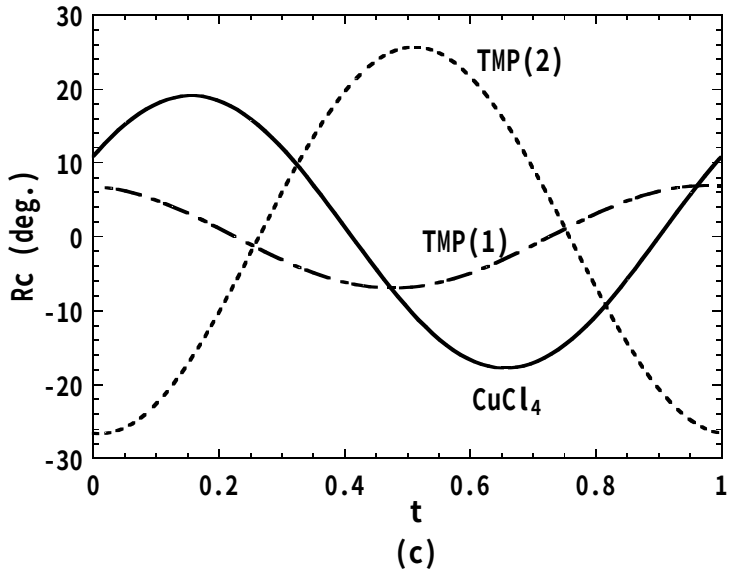
30
20
10
0
-10
-20
-30
Rc (deg.)
TMP(2)
TMP(1)
CuCl4
0
0.2
0.4
0.6
0.8
1
t
(c)

Fig. 4.

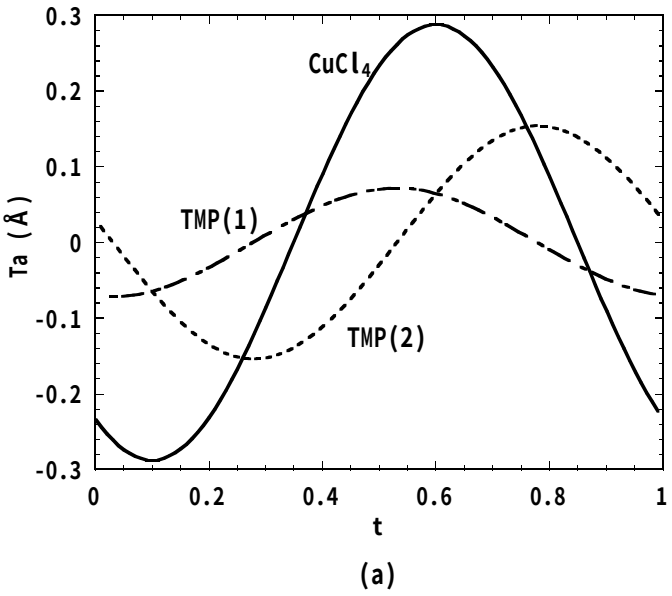
0.3
0.2
0.1
0
-0.1
-0.2
-0.3
Ta (Å)
CuCl4
TMP(1)
TMP(2)
0
0.2
0.4
0.6
0.8
1
t

(a)

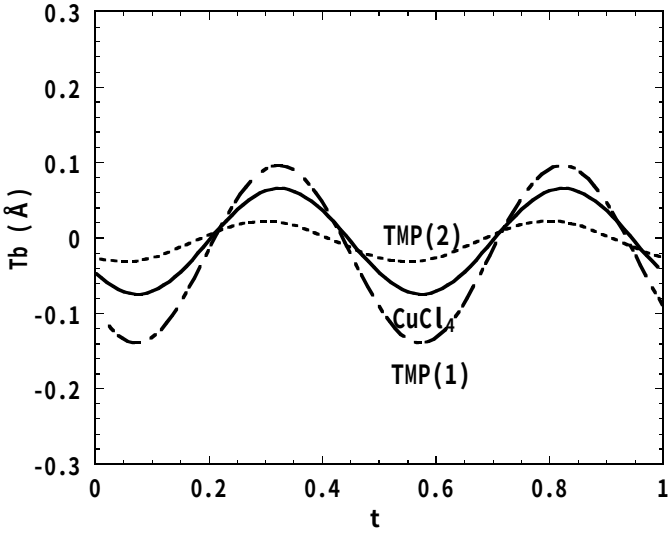
0.3
0.2
0.1
0
-0.1
-0.2
-0.3
Tb (Å)
TMP(2)
CuCl4
TMP(1)
0
0.2
0.4
0.6
0.8
1
t

(b)

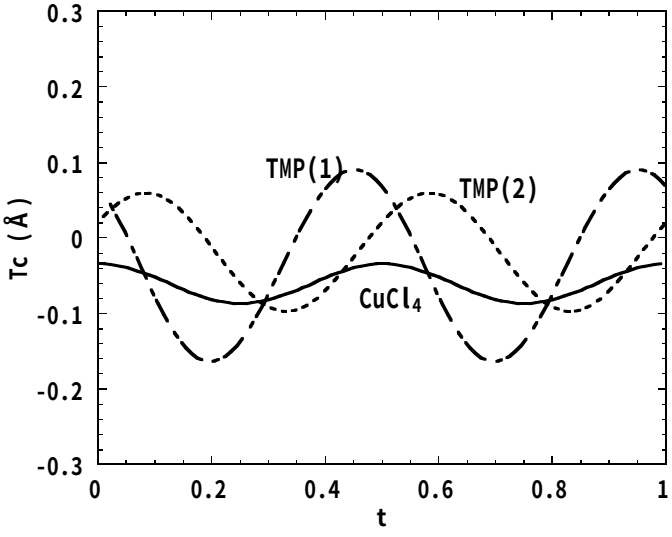
0.3
0.2
0.1
0
-0.1
-0.2
-0.3
Tc (Å)
TMP(1)
TMP(2)
CuCl4
0
0.2
0.4
0.6
0.8
1
t

(c)

Fig. 5.

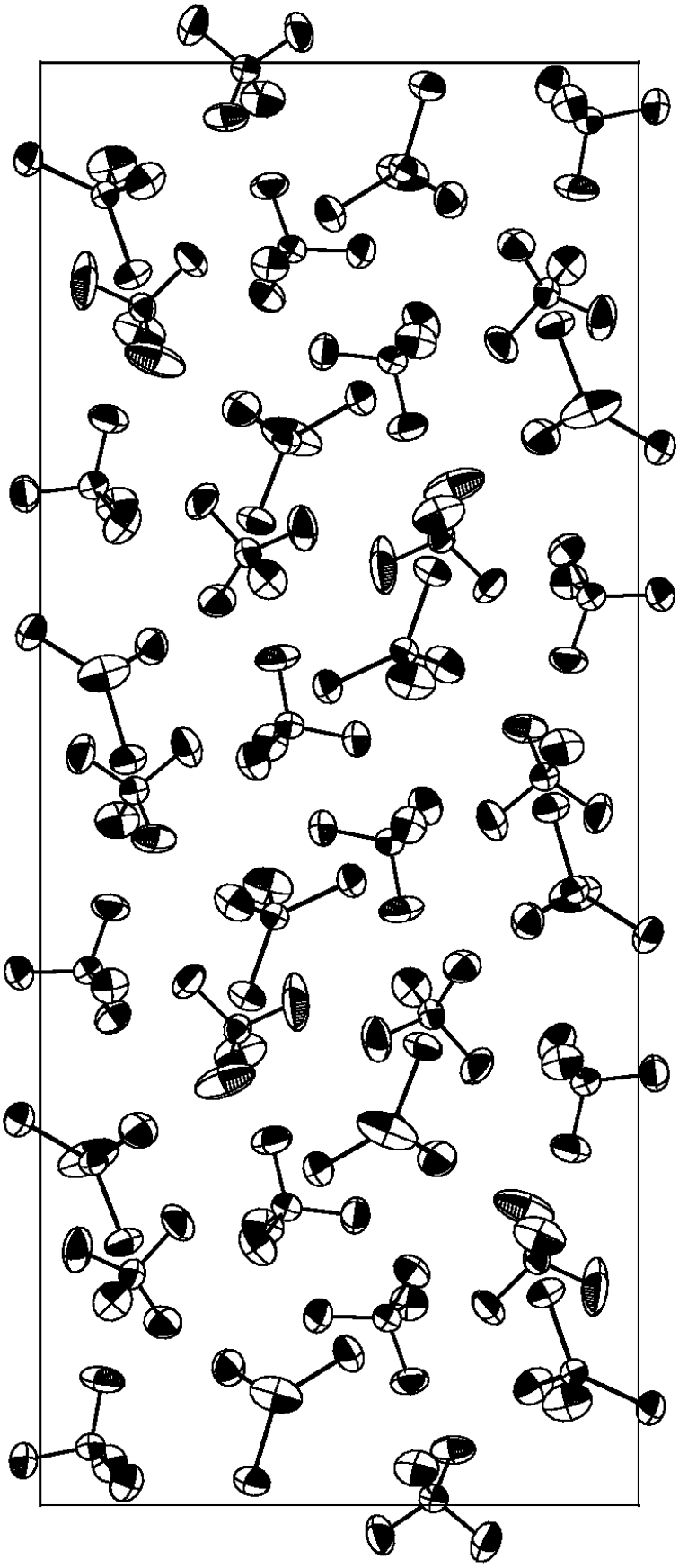

Fig. 6.

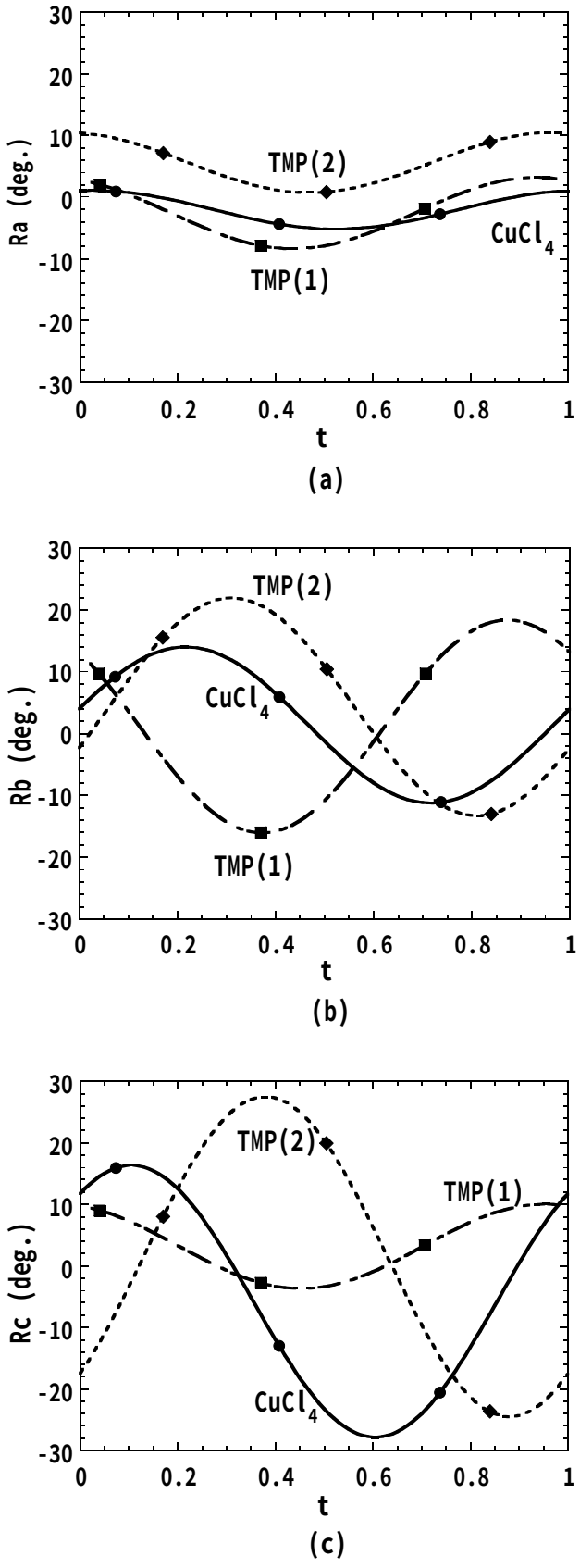
Ra (deg.)
TMP(2)
CuCl4
TMP(1)
t
(a)
Rb (deg.)
TMP(2)
CuCl4
TMP(1)
t
(b)
Rc (deg.)
TMP(2)
TMP(1)
CuCl4
t
(c)

Fig. 7.

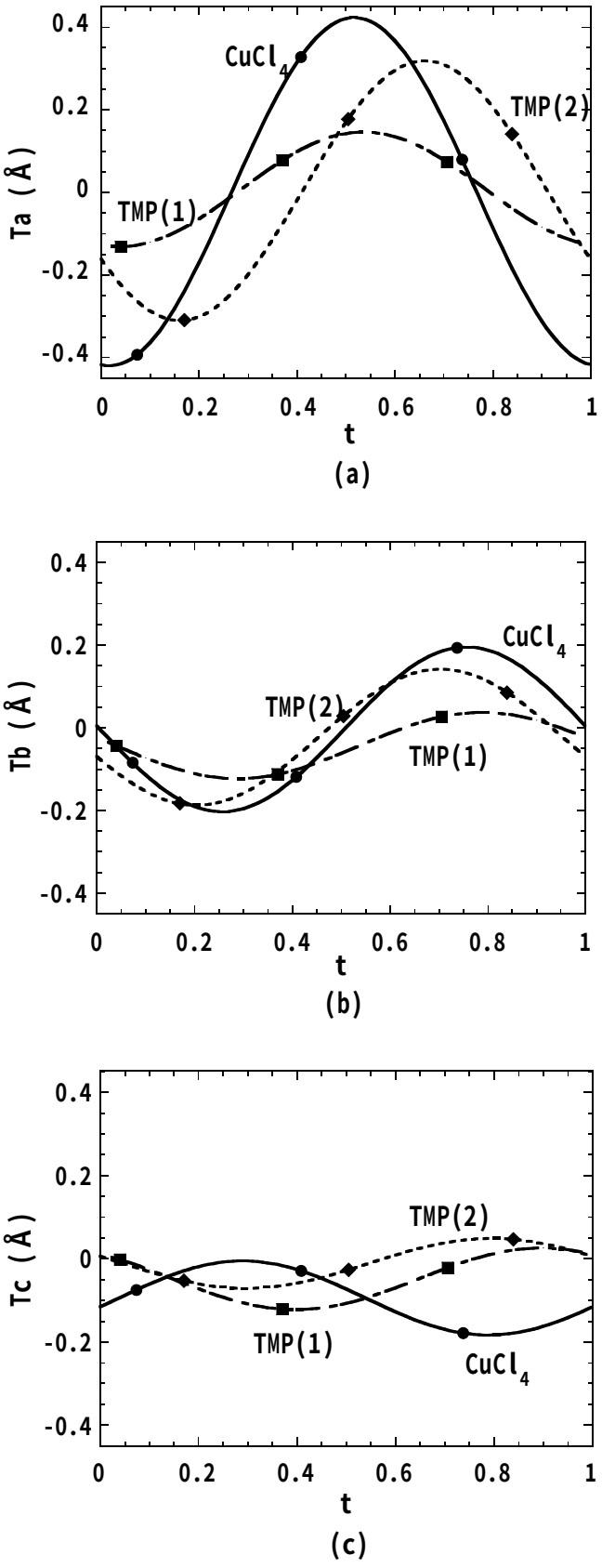
0.4
0.2
0
-0.2
-0.4
Ta (Å)
CuCl4
TMP(2)
TMP(1)
0
0.2
0.4
0.6
0.8
1
t
(a)
Tb (Å)
CuCl4
TMP(2)
TMP(1)
t
(b)
Tc (Å)
TMP(2)
TMP(1)
CuCl4
t
(c)

Fig. 8.